Faraday Discussions

Cite this: *Faraday Discuss.*, 2022, **237**, 389

PAPER

Impact of the terahertz and optical pump penetration depths on generated strain waves temporal profiles in a V_2O_3 thin film

Guénolé Huitric, [a] Michael Rodriguez-Fano,[b] Lucas Gournay,[a] Nicolas Godin,[ac] Marius Hervé, [a] Gaël Privault, [a] Julien Tranchant,[b] Zohra Khaldi,[b] Marco Cammarata, [a] Eric Collet, [ac] Etienne Janod[ac] and Christophe Odin *[ac]

Received 20th January 2022, Accepted 11th February 2022
DOI: 10.1039/d2fd00013j

Triggering new stable macroscopic orders in materials by ultrafast optical or terahertz pump pulses is a difficult challenge, complicated by the interplay between multiscale microscopic mechanisms, and macroscopic excitation profiles in samples. In particular, the differences between the two types of excitations are still unclear. In this article, we compare the optical response on acoustic timescale of a V_2O_3 Paramagnetic Metallic (PM) thin film excited by a terahertz (THz) pump or an optical pump, at room temperature. We show that the penetration depth of the deposited energy has a strong influence on the shape of the optical transmission signal, consistent with the modulation of permittivity by the superposition of depth-dependent static strain, and dynamical strain waves travelling back and forth in the sample layer. In particular, the temporal modulation of the optical transmission directly reflects the excitation profile as a function of depth, as well as the sign of the acoustic reflection coefficient between the film and the substrate. The acoustic mismatch between the V_2O_3 layer and the substrate was also measured. The raw data were interpreted with a one-dimensional analytical model, using three fitting parameters only. These results are discussed in the context of triggering phase transitions by ultrafast pump pulses. To the best of our knowledge, this is the first report of the modulation of the optical transmission of V_2O_3 with a THz pump within the acoustic timescale.

1. Introduction

The study of Photo-Induced Phase Transitions (PIPT) is in constant development, owing to new experimental techniques and progress in the physical and

[a]*Univ Rennes, CNRS, IPR (Institut de Physique de Rennes) – UMR 6251, F-35000 Rennes, France. E-mail: christophe.odin@univ-rennes1.fr*
[b]*Institut des Matériaux Jean Rouxel de Nantes (IMN), Univ Nantes, CNRS, F-44322 Nantes, France*
[c]*DYNACOM IRL2015 University of Tokyo - CNRS - UR1, Department of Chemistry, 7-3-1 Hongo, Tokyo 113-0033, Japan*

theoretical interpretation.[1] Moreover, the recent possibility to generate almost single cycle terahertz pulses of high intensity offers appealing perspectives for the excitation and investigation of coherent lattice vibrations.[2–6]

It was soon recognized that, in addition to the microscopic excitation mechanisms, the macroscopic excitation profile is also strikingly important both for the generation of new phases, their propagation in space and time, and for the interpretation of collected data. The finite penetration depth and hence excitation profile of the pump will induce an inhomogeneous distribution of phase nuclei from the surface,[7] which may propagate in the depth of the sample (for instance, photoinduced metallic domains in an insulating phase[8]). The initial spatial pattern is determined by the excitation profile and mechanism, and subsequent evolutions (nucleation, phase front propagation) are driven by corresponding spatial gradients. This spatial and dynamical mixture of sample properties modulates the sample dielectric function, whose effects are probed through time-resolved optical reflectivity or transmission measurements. A model of the full optical detection process was developed in the seminal work by Thomsen *et al.*,[9] pointing out the role and interplay between the pump and probe in the interpretation of the transient signal.

It is admitted that optical pump microscopic excitation processes are mainly mediated by electrons, while terahertz pulses can also interact directly with the lattice through infrared active phonon modes. Among possible transformations that are triggered by such ultrafast strong pulses are coherent phonons or strain-waves.[10,11] In

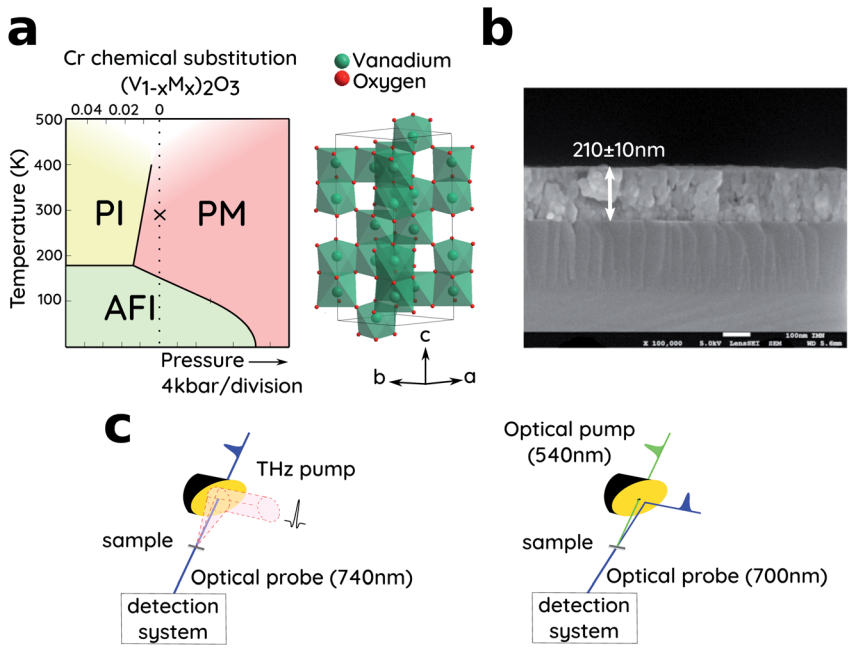

Fig. 1 (a) Phase diagram of V_2O_3 (PM: Paramagnetic Metal; PI: Paramagnetic Insulator; AFI: Antiferromagnetic Insulator) and structure in the PM phase. (b) Scanning Electron Microscope (SEM) image. The film thickness was measured as 210 ± 10 nm. (c) Experimental setups for the terahertz pump or optical pump/optical probe.

addition to possible applications to probe material properties, such strain waves were shown to be able to drive a semi-conductor to metal phase transition.[12]

For these reasons, the comparison of ultrafast pump properties is of primary importance in the understanding of PIPT phenomena, in particular in metal–insulator phase transitions of strongly correlated metals.

Vanadium sesquioxide V_2O_3 is a work horse in the study of Mott–Hubbard phase transitions.[13,14] At ambient pressure, it presents a first order symmetry-breaking Paramagnetic Metal (PM) to Antiferromagnetic Insulator (AFI) phase transition near 160 K, while a third phase (Paramagnetic Insulator, PI) can be obtained by changing pressure or chemical doping (Fig. 1a). At room temperature and pressure, V_2O_3 is in a paramagnetic correlated metallic phase, with a corundum structure with two V_2O_3 formula units in the rhombohedral $R\bar{3}c$ unit cell (Fig. 1a).

The ultrafast responses of such materials in pump–probe experiments are very important both for the understanding of the underlying physics and for potential applications. For instance, optical pump experiments have shown the possibility of inducing metallic nucleation-growth from the low-temperature insulating phase,[15] while very high terahertz-pump fields (>1 MV cm^{-1}) at 4 K achieved insulating to metal transition through electronic tunneling.[16]

In the following, we compare the optical relative transmission transients induced by a terahertz or an optical pump on a V_2O_3 thin film, using the same optical probe, to get information on photoinduced static and dynamical strains within the acoustic timescale.

2. Materials and methods

2.1 Sample preparation

A thin film of V_2O_3 was deposited on a c-cut (0001) sapphire substrate by sputtering of a vanadium target in Ar discharge. Post-deposition annealing at 530 °C in a reducing atmosphere yields a 210 ± 10 nm thick crystallized and single-phased V_2O_3 layer.

The sample thickness of 210 nm was chosen on the one hand because it is higher than the penetration depth of the optical pump (80 nm), and lower than that of THz pump (1300 nm) used in pump–probe experiments presented in this work. On the other hand, a thickness of 210 nm results in an optical density OD ≈ 1 (probe penetration depth is 95 nm), which usually provides a good contrast in ultrafast transmission measurements.

2.2 Experimental set-up and simulations

Schematics of the experimental setups are given in Fig. 1c where THz pump/optical probe and optical pump/optical probe techniques are used. The output of a femtosecond regenerative amplifier (Coherent) that delivers 100 fs pulses at 1 kHz repetition rate is split and used for both pump and probe beams. For the THz experiments, the main part (3 mJ) of the amplifier output is used to generate intense THz fields by optical rectification using the tilted-pulse-front technique[2,17] in $LiNbO_3$. We obtain a fluence of 1 μJ mm^{-2} and an electric field reaching 250 kV cm^{-1} (measured by Electro-Optical Sampling, EOS). The remaining output of the amplifier seeds an Optical Parametric Amplifier, OPA (TOPAS Light Conversion) in order to obtain the 740 nm pulse used as probe. The

photo-induced signal is recorded with a lock-in detection. For the optical pump experiment, we use the output of an OPA as pump. The wavelength is set to 540 nm and its fluence fixed to 35 μJ mm^{-2}. Due to experimental constraints, in this setup, a 700 nm probe wavelength is preferred. Both experiments are performed in transmission configuration at nearly normal incidence.

In this way, we measured the temporal relative variation of the optical transmission T_r, $\frac{\Delta T_r}{T_r} = [T_r(\text{on}) - T_r(\text{off})]/T_r(\text{off})$, where "on" and "off" mean respectively with and without pump. Eventually, a time-independent constant corresponding to the mean signal at negative times was subtracted. No other data treatments have been performed, nor any part of the signal removed.

Data reduction and all simulations were performed with home-made Python codes that use Numpy[18] and Scipy[19] libraries. Figures were drawn with Matplotlib.[20]

2.3 THz-time domain spectroscopy (TDS)

The V_2O_3 sample was characterized by terahertz time domain spectroscopy. The time traces of the THz electric field, measured by electro-optical sampling with a 1 mm thick ZnTe crystal, are shown in Fig. 2a. From their Fourier transforms, we extracted the complex dielectric function of the film using the Tinkham formula.[21–23] The mean absolute value of the transmission is $T \approx 0.375$, from which a static conductivity of $\sigma_o \approx 1000$ S cm^{-1} was calculated from the Tinkham formula.[21] This estimation is close to those obtained with the same types of samples by THz-TDS.[15,24–26] The frequency dependence of the real and imaginary parts of the dielectric function are shown in Fig. 2b, with the best fit using Drude's model for the conductivity, eqn 1

$$\varepsilon_\omega = \varepsilon_1 + i\varepsilon_2 = \varepsilon_\infty + i\frac{\sigma_\omega}{\omega\varepsilon_o} \quad \text{where} \quad \sigma_\omega = \frac{\sigma_o}{1 + i\omega\tau} \tag{1}$$

where ω is the angular frequency (rad s^{-1}), ε_o is the vacuum dielectric permittivity and ε_∞ the dielectric function at infinite frequency. We obtained an electronic scattering

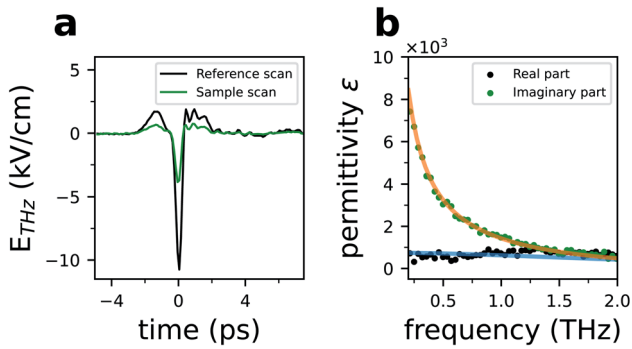

Fig. 2 Terahertz time domain spectroscopy of V_2O_3 at room temperature. (a) Electric field waveform as a function of time: bare substrate (reference scan) and substrate with thin film sample (sample scan). (b) Experimental real ε_1 and imaginary ε_2 parts of the dielectric function as a function of frequency. The continuous lines are the best fits using a Drude model.

rate $\Gamma = 1/\tau \approx 14.3 \pm 0.2$ THz, and a static conductivity of $\sigma_o \approx 1000$ S cm^{-1}. These values are consistent with those obtained in ref. 26 and 27. These parameters will be used in the following to calculate the sample refractive index at terahertz frequencies.

3. Results and analysis

3.1 Modulation of optical transmission by terahertz or optical pump

In the following we report the comparison of temporal relative transmission variation using either a THz pump or an optical pump. The THz pump EOS temporal trace, shown in Fig. 3c, has a maximum electric field ≈ 250 kV cm^{-1} and typical full duration ≈ 4 ps. The energy power spectrum has its maximum near 0.5 THz (Fig. 3d) with a full width at half maximum FWHM ≈ 0.5 THz. The optical pump at 540 nm has a duration of 100 fs. For experimental reasons, we could not use exactly the same probe wavelengths, 740 and 700 nm respectively for THz and optical pumps. However, it can be shown that the sensitivity function (see below Fig. 4) that determines how the probe interacts with the permittivity modulation induced by the pump are almost equal over the full film thickness, since the ratio

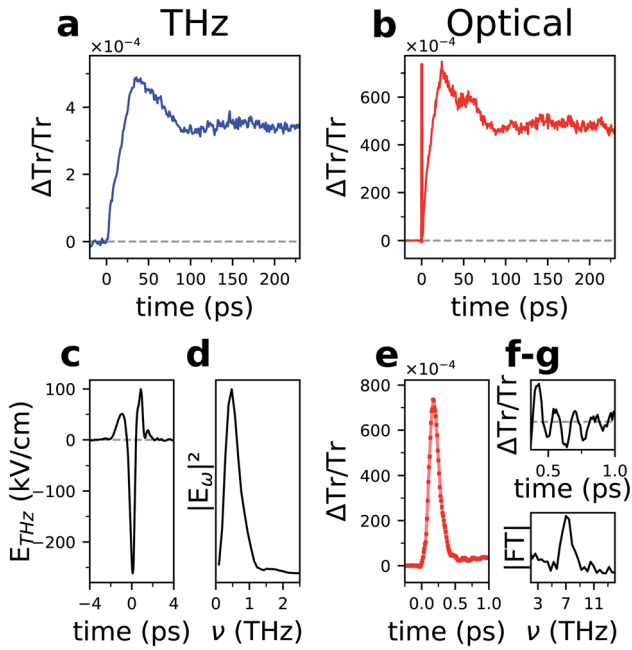

Fig. 3 (a and b) Relative optical transmission as a function of time $\frac{\Delta T_r(t)}{T_r}$. Raw data are presented. (a) THz pump. (b) Optical pump (540 nm). For $t \leq 1.5$ ps the time-step is 0.01 ps, while for $t \geq 2$ ps, the time-step is 0.5 ps. (c and d) Terahertz pump electric field waveform as a function of time, and corresponding squared modulus of the Fourier transform $|E_\omega|^2$. (e–g) Short-time analysis of the optical pump transmission acquisition shown in (b); (e) raw data (points) and best fit (continuous line); (f and g) evidence of coherent phonon excitation: (f) resulting transmission after subtraction of the peak and background as a function of time, and (g) the corresponding modulus of the Fourier transform.

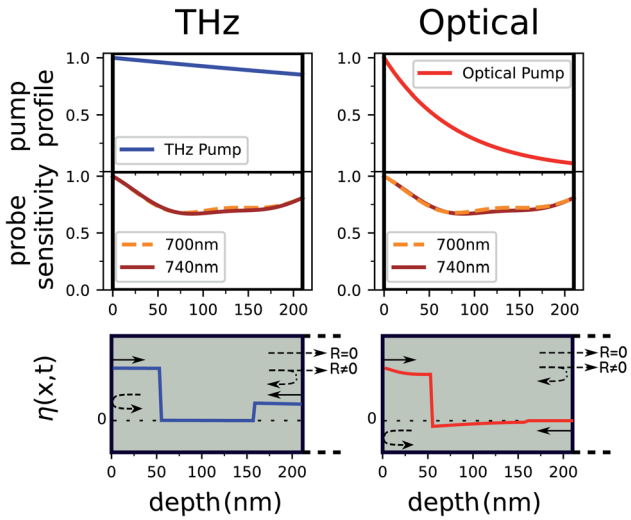

Fig. 4 Left: THz pump and right: optical pump. First line: excitation profiles and modulus of the sensitivity function in the thin film. Parameters correspond to the real parameters of the experiment. All functions were normalized to one at $x = 0$ for clarity. Second line: sketch of the thin-film and substrate interfaces and strain waves.

of the complex index to wavelength $\tilde{n}/\lambda$ are very close (difference of less than 6% for the real part, and 1% for the imaginary part).

The temporal evolution of the raw relative transmission variation $\frac{\Delta T_r(t)}{T_r}$ is presented on Fig. 3 for both pumps, with probes at almost the same wavelength.

Two features are immediately apparent. First, both signals increase within about 30 ps, reaching a maximum before decaying to an almost constant plateau value for delay times larger than 90 ps. In fact, for larger times, small oscillations modulate the plateau. For instance a bump appears near 150 ps in the terahertz pump profile. It is less clear for the optical pump profile. Second, the magnitude of the relative transmission variation with the optical pump is larger than the value with the terahertz pump, as expected from the largest available energy and fluence of the optical pulse.

Most significant is the difference in the profiles within the 35–90 ps time range. While the decay is rather uniform for the terahertz profile, a dip near 44 ps, and second maximum at 56 ps are clearly seen for the profile with the optical pump, making this profile strikingly different from the terahertz profile. Moreover, an additional strong sharp peak signal appears at very short time delays.

By noting that an acoustic timescale is the travel time of a wave from the top surface to the interface of the film with the substrate, that is in our case $\tau_a = d/v \approx$ 29 ps, and an electronic time-scale is typically a few 0.1 ps, we can split our analysis into two parts.

First, we analyse in more detail the optical short-time trace, which was studied with a shorter time-step of 0.01 ps, as presented in Fig. 3e. This photo-induced signal can be divided into three contributions. A first ultrafast response is located just after the pump arrival and lasts for less than 0.5 ps (see Fig. 3e). This

feature is related to the photon–electron interaction. At larger time delays, oscillations on a slowly growing background are perceptible. The extraction of the oscillating component is done by removing the two other contributions. The peak is fitted by the convolution of a Gaussian of full width at half height 120 fs, with an exponential decay of 80 fs time constant, while the increasing background is reproduced thanks to a first order polynomial. The Fourier transform of the remaining oscillating component unveils a 7.2 THz mode (see Fig. 3g), in accordance with the frequency of the A_{1g} optical phonon mode previously measured through Raman[28,29] and pump–probe experiments.[29–31] Concerning the THz pump experiment, neither the peak nor any oscillation were detected. The lack of oscillating component is due to the long THz excitation ($\sim$1 ps) compared to the period of the phonon mode ($\sim$0.14 ps), which washes out the oscillations due to the dephasing.

Second, as discussed before, for times larger than 1 ps, the features of the data fall in the acoustic timescale, the positions of peaks and dips corresponding more or less to multiples of the acoustic travel time $n \times \tau_a$ with n an integer. More precisely, we will show that the measured relative transmission variations as a function of time come from the modulation of the complex dielectric function by photo-induced elastic strain-waves. For metals, the strain waves are usually generated by a thermoelastic mechanism.[9–11,32] In this process, part of the pump pulse energy is absorbed by the electrons, which thermalize in a few hundreds of femtoseconds. During and after the pump pulse, the electronic and lattice degrees of freedom exchange energy through electron–phonon coupling and equilibrate to a common temperature, typically within less than a few picoseconds, a process that is usually described with a two-temperature model.[33] This almost instantaneous heating of the lattice, at the elastic timescale, induces an inhomogeneous thermal stress related to the pump energy deposition profile. The related strain modulates the dielectric function as a function of depth and time, giving rise to a time-dependent optical transmission variation.

In the following, we use the simplest one-dimensional model to interpret our data with the minimum number of fitting parameters.

3.2 Thermoelastic model

The relative transmission variation $\frac{\Delta T_r(t)}{T_r}$ depends both on the pump excitation profile that determines the strain pulse shape $\eta(x, t)$, and on the probe pulse transmission through the perturbed sample. The pioneering work of Thomsen *et al.*[9] with a semi-infinite sample was generalized to a multilayer system by Matsuda *et al.*[34]

In the following, we consider a layer of thickness d on top of a semi-infinite substrate (Fig. 4). Note however that a more complete model, with a finite-width substrate, gives identical results.

Assuming that the permittivity, or refractive index, is modulated by the strain, and using the approximation $\Delta\tilde{n}(x,t) = \frac{\partial\tilde{n}}{\partial\eta}\eta(x,t)$, the relative change of transmission can be written as:

$$\frac{\Delta T_r(t)}{T_r} = \Re\mathrm{e}\left(\frac{\partial\tilde{n}}{\partial\eta}\int_0^d \eta(x,t)\tilde{f}\left(x,\lambda_{pr},\tilde{n},\tilde{n}_s,d\right)\mathrm{d}x\right) \quad (2)$$

Table 1 Parameters used in the simulations. $i^2 = -1$

Parameter	Value	References
Al_2O_3 (sapphire)		
ρ	3.98 g cm^{-3}	
v_{001} (sound velocity)	11.23 × 10^5 cm s^{-1}	Winey *et al.*[35]
Z_s (acoustic impedance)	44.7 × 10^5 g cm^{-2} s^{-1}	
n (visible)	1.76	Tropf *et al.*[36]
n (THz)	3.07	Grischkowsky *et al.*[37]
V_2O_3 (PM)		
ρ	4.87 g cm^{-3}	
v_{100} (sound velocity)	7.37 × 10^5 cm s^{-1}	Yelon and Keem[38]
Z (acoustic impedance)	35.9 × 10^5 g cm^{-2} s^{-1}	
$\tilde{n}$ @ 540 nm	1.73 + 0.54 i	Qazilbash *et al.*[39]
$\tilde{n}$ @ 700 nm	1.74 + 0.58 i	Qazilbash *et al.*[39]
$\tilde{n}$ @ 740 nm	1.72 + 0.61 i	Qazilbash *et al.*[39]
ξ_{THz}	1300 nm	From THz-TDS
ν_p (Poisson coefficient)	0.33	
C_p (heat capacity)	3.25 J K^{-1} cm^{-3}	Keer *et al.*[40]

where $\Re\mathfrak{e}$ stands for the real part of a complex number, and $\tilde{f}(x, \lambda_{pr}, \tilde{n}, \tilde{n}_s, d)$ is a complex-valued "sensitivity function".[9] This sensitivity function describes the interaction of the probe with the permittivity modulation, and accounts for both absorption and interference effects. The parameters are the probe wavelength λ_{pr}, the film and substrate complex refractive indexes $\tilde{n}$ and $\tilde{n}_s$, and the film thickness d. All these values are known either from the literature or direct measurement (see Table 1).

In this equation, we made the assumption that the derivative of the film photoelastic complex constant $\frac{\partial \tilde{n}}{\partial \eta}$ is not a function of depth. It is an unknown that can only be estimated by fitting the data.

The strain profile $\eta(x,t) = \frac{\partial u(x,t)}{\partial x}$, where $u(x, t)$ is the displacement, can be obtained by solving the two coupled elastic-wave equations:

$$\frac{\partial^2 u}{\partial t^2} = v^2 \frac{\partial^2 u}{\partial x^2} - v^2 \frac{\partial \eta_{th}}{\partial x} \quad \text{for } 0 \le x \le d \tag{3}$$

$$\frac{\partial^2 u_s}{\partial t^2} = {v_s}^2 \frac{\partial^2 u_s}{\partial x^2} \quad \text{for } x > d \tag{4}$$

The subscript s indicates the substrate. The last term in right side of the first equation is the thermal strain, defined as:

$$\eta_{th}(x,t) = \eta_o \exp\left(-x/\xi_{pump}\right)\Theta(t), \quad \eta_o = \beta_T \Delta T_o \frac{1+\nu_p}{1-\nu_p} \tag{5}$$

$\Theta(t)$ is the Heaviside function, ξ_{pump} the pump penetration depth, β_T the linear expansion coefficient, ΔT_o the initial lattice maximum temperature rise at the surface, and ν_p the film Poisson ratio. The validity domain of such a system of equations is discussed for instance in ref. 9 and 10. The initial temperature jump is

related to pump fluence F_p, intensity reflection coefficient R_p and sample heat capacity per unit volume C, by the formula $\Delta T_o = \frac{(1-R_p)F_p}{C\xi_{pump}}$. It is worth mentioning however that the details of the energy exchange mechanisms that produce the initial stress on the lattice, are not important in this model, as long as the initial photoinduced lattice perturbation is very fast compared to the acoustic timescale, leading to an approximate stepwise temporal rise.

Thus, four dimensionless parameters determine the solutions. First, the strain wave reflection coefficient R defined as

$$R = \frac{Z_s - Z}{Z_s + Z} \tag{6}$$

where Z_s and Z are respectively the substrate and thin film acoustic impedances ($Z = \rho v$ with ρ the density and v the sound velocity). Second the ratio $K = \frac{d}{\xi_{pump}}$ of the film thickness d and the pump penetration depth ξ_{pump}. If $K \ll 1$, the excitation profile is almost constant within the film, whereas the exponential decay is strongly marked when $K \gg 1$. Third, $V = \frac{v}{v_s}$ the ratio of sound velocities in the layer and the substrate. And finally the strain at the top-layer surface η_o.

Using Laplace transforms methods, the solutions of eqn (4), $u(x, t)$ and $\eta(x, t)$ in the film and the substrate, were calculated analytically, with the initial conditions of no displacement and strain, as well as zero velocity at $t = 0$, boundary conditions of continuous displacement and stress at the film–substrate interface, and free surface at the air-layer interface (zero-stress condition).

Thus, by combining the solutions of eqn (4), and the formula eqn (2), it is possible to simulate and fit the data, as explained below.

We show in Fig. 4 the normalized excitation profiles for the two pumps and sensitivity functions at the two probe wavelengths, using values from Table 1. As expected, the terahertz excitation is almost constant over the whole film thickness ($\xi_{THz} = 1300$ nm), in contrast to the optical excitation that has a penetration depth of $\xi_{540nm} = 80$ nm. As already said above, the probe sensitivity functions $\tilde{f}(x, \lambda_{pr}, \tilde{n}, \tilde{n}_s, d)$ are very close to each other, and the difference has a negligible effect on the transmission. Thus, we can conclude that if a change of transmission is observed, it is a consequence of the different pump excitations. Interestingly, we also note that the probe sensitivity function is almost constant, despite the $\xi_{probe} = 95$ nm penetration depth of the 700 nm or 740 nm probes. This is a consequence of finite size thickness that leads to constructive interferences within the film.

To get further insight into the interpretation of the data $\frac{\Delta T_r(t)}{T_r}$, we first discuss a rough approximation of eqn (2). Assuming a constant complex-valued sensitivity function $\tilde{f}(x,\ldots) = \tilde{f}(\ldots)$, eqn (2) can be easily simplified to:

$$\frac{\Delta T_r(t)}{T_r} \approx \Re e\left(\frac{\partial \tilde{n}}{\partial \eta}\tilde{f}(\ldots)\int_0^d \eta(x,t)\mathrm{d}x\right) = \Re e\left(\frac{\partial \tilde{n}}{\partial \eta}\tilde{f}(\ldots)\right)\int_0^d \frac{\partial u(x,t)}{\partial x}\mathrm{d}x$$

Thus

$$\frac{\Delta T_r(t)}{T_r} \approx \Re e\left(\frac{\partial \tilde{n}}{\partial \eta}\,\tilde{f}(\ldots)\right)[u(d,t)-u(0,t)] = \Im \Delta u(t) \quad (7)$$

where $\Delta u(t) = u(d,t) - u(0,t)$ and $\Im = \Re e\left(\frac{\partial \tilde{n}}{\partial \eta}\,\tilde{f}(\ldots)\right)$. Within this approximation, the relative transmission variation is simply proportional to the variation of the film thickness $\Delta u(t)$.

The behaviour of $\Delta u(t)$ for both terahertz and optical pumps, as well as snapshots of the strain profile $\eta(x, t)$ at typical times, is illustrated in Fig. 5, using values from Table 1, and three values of the strain reflection coefficient $R = 0$ (matched layer), $R = \pm 0.2$. The behaviour of the strain spatial profile is interesting (Fig. 5c and d),

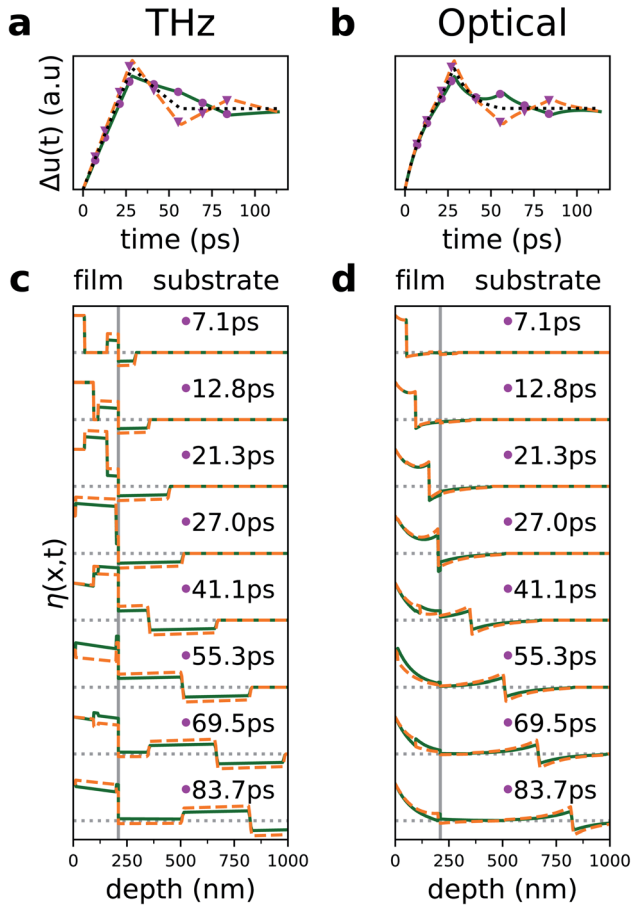

Fig. 5 Temporal evolution of $\Delta u(t)$ (a and b) and snapshots of the strain profile $\eta(x, t)$ (c and d) within the film and the substrate as a function of position at some selected times. Left column (a and c) and right columns (b and d) correspond respectively to THz and optical pump. Panels a and b represent $\Delta u(t)$ with matched layer $R = 0$ (black dotted line) or unmatched $R = \pm 0.2$ ($R = -0.2$ orange dashed line and $R = +0.2$ green continuous line). Markers are placed at times at which corresponding strain wave snapshots are plotted as a function of position. Panels c and d: strain wave profiles $\eta(x, t)$ in the thin film (left of the vertical black line) or in the substrate (right of the vertical black line) at a given time, as a function of position. Horizontal dotted gray lines represent zero strain $\eta = 0$ line for each time. For the simulation, the sound velocity in the substrate was set to 1.5ν.

and can be understood using three contributions. A time-independent contribution corresponding to the initial temperature profile, and propagating and counter-propagating strain waves launched at the free surface and film–substrate surface by the initial stress impulse. The resulting strain is the sum of these three contributions, and evolves depending on the reflections at the free surface or film–substrate interface. At each reflection on the film–substrate interface, the amplitude of the strain-wave is multiplied by R, resulting in a magnitude after n round trips of duration $2\tau_a = 2d/v$ reduced by a factor R^n. For times $\gg 2n\tau_a$ long enough such that $R^n \ll 1$, only the time-independent strain (static strain) survives. Thus, we expect the time-independent strain to determine the magnitude of the plateau. Of course, other phenomena are susceptible to modulate the shape of the transmission signal. For instance, the static strain being related to a temperature profile, and thus to a temperature gradient, heat diffusion, loss and transfer, will smooth and wash away the temperature gradient, and strain, until thermodynamical equilibrium is reached. Such phenomena are negligible on the studied timescale, and are not taken into account in this model.

As remarked by Schick *et al.*[41] who treated the case of a matched layer $R = 0$, the full strain presents positive and negative contributions in the limit $d \gg \xi_{pump}$. In the opposite limit $d \ll \xi_{pump}$, the strain has almost the same sign over all the film thickness. It was explained by the fact that the static strain always compensates the strain wave. This conclusion remains valid in our model, at least for the small considered reflection coefficient magnitude $|R| < 0.2$.

Clearly, a comparison of the simulations shown in Fig. 5a and b with the raw data of Fig. 3 shows that the studied V_2O_3 film is not matched to the sapphire substrate. If the layer were matched, $\Delta u(t)$ would reach a plateau after the strain wave launched at the film–substrate interface has travelled back and forth in the film, that is $2\tau_a = 2d/v \approx 58$ ps (black dotted lines of Fig. 5a and b). But experimental data show a variation over more than 90 ps. Considering now the unmatched case, we can determine the sign of the reflection coefficient. For $R < 0$, a dip below the plateau value appears near time $2\tau_a$, which is inconsistent with Fig. 3. Thus we conclude that R is positive, $R > 0$, meaning that the sapphire acoustic impedance is larger than the one of the V_2O_3 film, $Z_s > Z$.

3.3 Analysis

To go further in the analysis of the data, we fitted data obtained from the terahertz and optical pumps with this simplest possible model using the full eqn (2), and the analytical solution of eqn (4).

First, the terahertz penetration depth deserves particular attention, because of the frequency distribution of energy $|E_\omega|^2$ of the terahertz excitation pump pulse, shown in Fig. 6.

From the optical conductivity measured by TDS, and Drude's formula eqn (1), we calculated the complex refractive index (real and imaginary parts in Fig. 6a), and penetration depth $1/\alpha_\omega$ (Fig. 6b). As shown by the figures, these parameters strongly depend on frequency, giving rise to the question of choosing an effective penetration depth in the formula. We model the intensity absorption profile by a weighted average of the absorption profile at each frequency

$$I(x) \sim \int \mathrm{d}\omega P_\omega \alpha_\omega \mathrm{e}^{-\alpha_\omega x} \sim \frac{1}{\xi_{THz}} \mathrm{e}^{-x/\xi_{THz}} \tag{8}$$

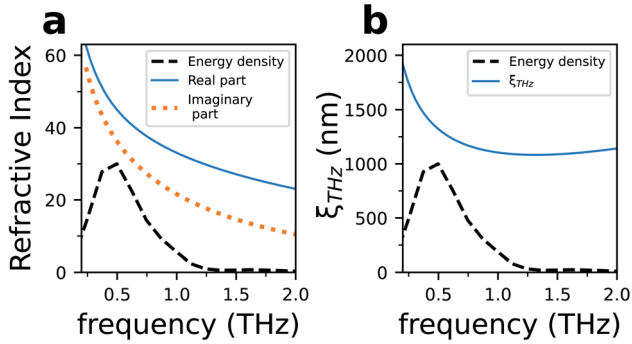

Fig. 6 (a) Real and imaginary parts of the thin film complex index at THz frequencies, as given by the TDS experiment. (b) Corresponding THz penetration depth as a function of frequency. The dashed line represents the terahertz pump pulse spectral density $|E_\omega|^2$ with arbitrary unit.

with probability P_ω of absorbing energy within ω and $\omega + \mathrm{d}\omega$ defined as

$$P_\omega = \frac{|E_\omega|^2}{\int \mathrm{d}\omega |E_\omega|^2}$$

From the numerical integration of eqn (8), we obtained the effective penetration depth for the terahertz pump $\xi_{\mathrm{THz}} \approx 1300$ nm. In fact, the mean absorption profile is almost indistinguishable to the one at single frequency 0.5 THz over all film thickness.

Second, among the fitting parameters, the photoelastic constants $\frac{\partial n}{\partial \eta}$ and $\frac{\partial \kappa}{\partial \eta}$, where n and κ are respectively the real and imaginary parts of the complex refractive index $\tilde{n}$, are usually difficult to estimate. We tried to fit these parameters to our data, without success. But as already mentioned before, the fact that the sensitivity-function is almost depth independent combines the photoelastic constants with the scaling factor, making it difficult or impossible to distinguish both parameters that are strongly correlated. We also verified that a change of the photoelastic constants values could be almost compensated by a change of the scaling factor. Thus, we choose to separate the magnitude from the phase as $\frac{\partial \tilde{n}}{\partial \eta} = \left|\frac{\partial \tilde{n}}{\partial \eta}\right| \mathrm{e}^{-\mathrm{i}\phi_n}$. The photoelastic magnitude $\left|\frac{\partial \tilde{n}}{\partial \eta}\right|$ is incorporated to the overall scaling factor, while the phase ϕ_n was calculated from the relationship $\frac{\partial n}{\partial \eta} = -1.63 \frac{\partial \kappa}{\partial \eta}$ that was used in ref. 24 and 25.

Therefore, we ended with only three fitting parameters: the acoustic reflection coefficient R, and two scaling factors to adjust the amplitudes to the terahertz or optical-pump results. All the other parameters were obtained from the literature or measured in the laboratory, and fixed to the corresponding values (Table 1).

The best fit is presented in Fig. 7, and shows an overall very good agreement with the data for a three-parameter fit. We would like to stress again that the model fits the overall relative optical transmission variation data without any other corrections, including the rising, decreasing and pseudo-plateau parts. In particular, the result of the exponential excitation profile of the optical pump is well reproduced, as well as the small oscillation coming from the reflection of the

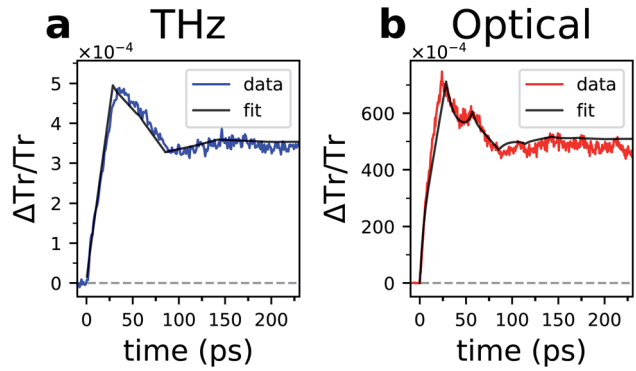

Fig. 7 Relative optical transmission as a function of time $\frac{\Delta T_r(t)}{T_r}$, and best fit results with only three parameters. Experimental raw data are presented. (a) THz pump. (b) Optical pump. Only points every 0.5 ps are shown.

strain pulse at the film–substrate interface. Interestingly, for the optical pump, it shows that the round shape of the rising part when time < 25 ps is also given by the exponential excitation profile, in addition to other possible mechanisms such as non-instantaneous heating, heat diffusion or loss, that are not taken into account in the model.

The value of the fitted acoustic reflection coefficient $R \approx 0.18 \pm 0.02$ is larger than the expected value $R \approx 0.11$ calculated from densities and sound velocities extracted from the literature (Table 1). From R, we obtain the ratio of substrate to film acoustic impedance $Z_s/Z \approx 1.44$. It gives an effective acoustic impedance of V_2O_3 of $Z \approx 31.0 \times 10^5$ g cm^{-2} s^{-1} instead of $Z \approx 35.9 \times 10^5$ g cm^{-2} s^{-1} using density and sound velocity along (110) from the literature, since our sample has a preferential orientation along (110). This small discrepancy of −14% may have different origins.

First, a density change due to internal stress/strain created during the synthesis process might be invoked. However, such effects are usually smaller than 1% in V_2O_3 films (see *e.g.* ref. 42) and cannot account for the observed 14% differences in R values.

Second, values from the literature come usually from single crystal samples that cannot be directly compared to thin films. As a matter of fact, the thin film sample has a heterogeneous structure, with typical grain sizes estimated to be around 25–30 nm, as revealed by the SEM image of Fig. 1b. This dense mixture of nanocrystals introduces orientational disorder, and changes the effective density because of the presence of holes or porosity. Different orientations correspond to different elastic constants and sound velocities. As a result, the measurement over the beamsize would give an effective acoustic impedance by spatial averaging. For instance, in disordered inhomogeneous systems,[43] an effective density and elastic stiffness are obtained by averaging the density, and the inverse of the elastic stiffness. It results in an effective sound velocity that can be smaller than the components' velocities. In our case, the presence of holes or less dense components decreases the effective density, and thus the acoustic impedance.

4. Discussion and conclusion

In this article, the role of the pump profile on the temporal evolution of the ultrafast optical time-resolved transmission response of a thin film of vanadium sesquioxide in the metallic phase was studied for two types of pumps: a terahertz pump and an optical pump. Using raw relative transmission data and only three fitting parameters, the temporal profile of the relative optical transmission for both pumps was analysed within the thermoelastic framework over a 250 ps time range, corresponding to the acoustic timescale of this V_2O_3 film.

From the material point of view, we also measured the acoustic impedance mismatch between the V_2O_3 film and sapphire substrate ($R \approx 0.2$). Such a mismatch was unexpected, and gives another important control parameter in addition to usual ones (X-rays diffraction, four-points resistivity measurements, SEM…), to improve the synthesis methodology and better control the quality of the films in the design of new electronic or opto-electronic devices.

We evidenced that the terahertz absorption profile is almost homogeneous over the film thickness (large penetration depth compared to film thickness). Conversely, the optical pump presents a marked exponential decay within the sample whose shape governs the transmission temporal profile at all times. These differences in excitation profiles are directly observed on the shape of the transmission transients. We showed that the superposition of strain waves to the static strain plays a central role in the interpretation of the data, the former having a contribution that decreases as time increases, the latter determining the plateau value within the acoustic timescale, and for time much smaller than heat transfer timescales. The crucial step in the data interpretation was to use full raw relative optical transmission data with no time-varying "background" removal. Note also that the transmission sensitivity function being almost flat, it can catch the effect of static strain and dynamical contribution with a small distortion, in contrast to reflectivity sensitivity functions.

Among the few studies of the transmission of V_2O_3 in the PM phase near room temperature, we only found one dealing with a terahertz pump and an optical probe, Giorgianni *et al.*[16] However, the transmission data were acquired over a very short time <6 ps, at 175 K, and with a very high field (>1 MV cm^{-1}), making comparison with our data impossible.

Liu *et al.*[24] studied a 400 nm thick V_2O_3 film at 220 K, with an optical pump and terahertz probe within 250 ps, and interpreted the data with a constant sensitivity function. The results are shown in the supplementary material of their article, where two acoustic echoes were evidenced. Similar results, but with a reflectivity setup $\Delta R/R$ and optical pumps, were also presented by Abreu *et al.*[25] and Mansart *et al.*[30] Note that all these authors only presented the oscillatory part of the signal after removal of some time varying background. We would like to point out that the extraction of the "oscillating" contributions may obscure the presence or absence of the contribution of a static strain. Our analysis demonstrated the importance of this static strain in the interpretation of the plateau observed for both excitation processes.

Recently, a comparison of coherent acoustic phonon generation by terahertz and near infrared ultrashort pump pulses (1.55 eV) on chromium metallic thin film ($\approx$14 nm) with the same probe wavelength (400 nm) was carried out.[32] It is

demonstrated that terahertz pulse pumping in metals generates coherent phonons by a thermoelastic process, through an ultrafast Joule effect. For the optical pump, this process arises by an intraband hot electron relaxation by heat transfer to the lattice degrees of freedom. Although the mechanisms differ, the oscillatory parts of the transient optical transmissions overlap almost perfectly, within the experimental time range <30 ps, suggesting similar response of the thin metallic film to both excitation processes. In contrast, our observations with a much thicker thin film of V_2O_3, and on much longer times, were clearly able to distinguish between the response to the terahertz and optical pump excitations.

For controlling materials at the macroscopic scale with strong ultrafast pulses, the strain–stress profile is a key feature, and we have shown that terahertz or optical pumps generate different profiles. With this respect, terahertz excitation allows for inducing a more spatially homogeneous excitation over the film depth than optical pump. Thus, we expect thermalization effects that depend on temperature gradients $\frac{\partial T}{\partial x}$ to be minimized. Moreover, in agreement with the matched layer model,[41] our unmatched layer model also predicts that the strain does not change sign when the excitation is almost uniform over the full film thickness, at least in the range $|R| < 0.2$ of our simulations, whereas tensile and compressive strain develop inhomogeneously in the film thickness when the intensity decreases exponentially. This change of sign of the strain, or not, within the sample may be of importance in the study of PIPT where the strain or stress-waves are at the origin of the driving mechanisms that trigger the phase transformation. The comprehension of such phenomena may help in tailoring strain profiles to study ultrafast phase transformations of volume changing materials such as V_2O_3.

Author contributions

GH and CO supervised the project. GH performed pump–probe and THz-TDS experiments. Technical support has been provided by NG, LG, GP, MH and CO prior and during experiments. GH and CO performed data analysis. CO developed the analytical model and carried out the simulations. MR, ZK, JT and EJ synthesized and characterized the sample. MC initiated the THz project and designed the THz setup. LG built the THz source during his PhD thesis. Financial support has been provided by EC and MC. CO and GH wrote the manuscript, with critical reading from EC and EJ. All authors contributed to discussions.

Conflicts of interest

There are no conflicts to declare.

Acknowledgements

The authors gratefully acknowledge Agence Nationale de la Recherche for financial support under grant, ANR-19-CE30-0004 ELECTROPHONE, ANR-19-CE29-0018 MULTICROSS, the University Rennes 1 and CNRS Human Resources Direction, for funding. We acknowledge Maciej Lorenc and Roman Bertoni for

experimental support, and fruitful discussions. We would like to thank Pr. H. Cailleau, and Céline Mariette, for useful discussions.

Notes and references

1 S. Koshihara, T. Ishikawa, Y. Okimoto, K. Onda, R. Fukaya, M. Hada, Y. Hayashi, S. Ishihara and T. Luty, *Phys. Rep.*, 2022, **942**, 1–61.
2 H. Hirori, A. Doi, F. Blanchard and K. Tanaka, *Appl. Phys. Lett.*, 2011, **98**, 091106.
3 P. Salén, M. Basini, S. Bonetti, J. Hebling, M. Krasilnikov, A. Y. Nikitin, G. Shamuilov, Z. Tibai, V. Zhaunerchyk and V. Goryashko, *Phys. Rep.*, 2019, **836–837**, 1–74.
4 C. Vicario, M. Jazbinsek, A. V. Ovchinnikov, O. V. Chefonov, S. I. Ashitkov, M. B. Agranat and C. P. Hauri, *Opt. Express*, 2015, **23**, 4573–4580.
5 T. Kampfrath, K. Tanaka and K. A. Nelson, *Nat. Photonics*, 2013, **7**, 680–690.
6 D. Nicoletti and A. Cavalleri, *Adv. Opt. Photonics*, 2016, **8**, 401–464.
7 H. Okamoto, Y. Ishige, S. Tanaka, H. Kishida, S. Iwai and Y. Tokura, *Phys. Rev. B: Condens. Matter Mater. Phys.*, 2004, **70**, 165202.
8 Y. Okimoto, X. Peng, M. Tamura, T. Morita, K. Onda, T. Ishikawa, S. Koshihara, N. Todoroki, T. Kyomen and M. Itoh, *Phys. Rev. Lett.*, 2009, **103**, 027402.
9 C. Thomsen, H. T. Grahn, H. J. Maris and J. Tauc, *Phys. Rev. B: Condens. Matter Mater. Phys.*, 1986, **34**, 4129–4138.
10 O. Matsuda, M. C. Larciprete, R. Li Voti and O. B. Wright, *Ultrasonics*, 2015, **56**, 3–20.
11 P. Ruello and V. E. Gusev, *Ultrasonics*, 2015, **56**, 21–35.
12 C. Mariette, M. Lorenc, H. Cailleau, E. Collet, L. Guérin, A. Volte, E. Trzop, R. Bertoni, X. Dong, B. Lépine, *et al.*, *Nat. Commun.*, 2021, **12**, 1239.
13 N. F. Mott and R. Peierls, *Proc. Phys. Soc.*, 1937, **49**, 72–73.
14 P. Hansmann, A. Toschi, G. Sangiovanni, T. Saha-Dasgupta, S. Lupi, M. Marsi and K. Held, *Phys. Status Solidi B*, 2013, **250**, 1251–1264.
15 E. Abreu, S. Wang, J. G. Ramírez, M. Liu, J. Zhang, K. Geng, I. K. Schuller and R. D. Averitt, *Phys. Rev. B*, 2015, **92**, 085130.
16 F. Giorgianni, J. Sakai and S. Lupi, *Nat. Commun.*, 2019, **10**, 1159.
17 K.-L. Yeh, M. Hoffmann, J. Hebling and K. A. Nelson, *Appl. Phys. Lett.*, 2007, **90**, 171121.
18 C. R. Harris, K. J. Millman, S. J. van der Walt, R. Gommers, P. Virtanen, D. Cournapeau, E. Wieser, J. Taylor, S. Berg, N. J. Smith, R. Kern, M. Picus, S. Hoyer, M. H. van Kerkwijk, M. Brett, A. Haldane, J. F. del Río, M. Wiebe, P. Peterson, P. Gérard-Marchant, K. Sheppard, T. Reddy, W. Weckesser, H. Abbasi, C. Gohlke and T. E. Oliphant, *Nature*, 2020, **585**, 357–362.
19 P. Virtanen, R. Gommers, T. E. Oliphant, M. Haberland, T. Reddy, D. Cournapeau, E. Burovski, P. Peterson, W. Weckesser, J. Bright, S. J. van der Walt, M. Brett, J. Wilson, K. J. Millman, N. Mayorov, A. R. J. Nelson, E. Jones, R. Kern, E. Larson, C. J. Carey, İ. Polat, Y. Feng, E. W. Moore, J. VanderPlas, D. Laxalde, J. Perktold, R. Cimrman, I. Henriksen, E. A. Quintero, C. R. Harris, A. M. Archibald, A. H. Ribeiro, F. Pedregosa, P. van Mulbregt and SciPy 1.0 Contributors, *Nat. Methods*, 2020, **17**, 261–272.
20 J. D. Hunter, *Comput. Sci. Eng.*, 2007, **9**, 90–95.
21 R. Glover III and M. Tinkham, *Phys. Rev.*, 1957, **108**, 243.

22 P. U. Jepsen, D. G. Cooke and M. Koch, *Laser Photonics Rev.*, 2011, **5**, 124–166.
23 J. Neu and C. A. Schmuttenmaer, *J. Appl. Phys.*, 2018, **124**, 231101.
24 M. K. Liu, B. Pardo, J. Zhang, M. M. Qazilbash, S. J. Yun, Z. Fei, J.-H. Shin, H.-T. Kim, D. N. Basov and R. D. Averitt, *Phys. Rev. Lett.*, 2011, **107**, 066403.
25 E. Abreu, S. N. Gilbert Corder, S. J. Yun, S. Wang, J. G. Ramírez, K. West, J. Zhang, S. Kittiwatanakul, I. K. Schuller, J. Lu, S. A. Wolf, H.-T. Kim, M. Liu and R. D. Averitt, *Phys. Rev. B*, 2017, **96**, 094309.
26 Y. Luo, F. Su, C. Zhang, L. Zhong, S. Pan, S. Xu, H. Wang, J. Dai and G. Li, *Opt. Commun.*, 2017, **387**, 385–389.
27 I. Lo Vecchio, L. Baldassarre, F. D'Apuzzo, O. Limaj, D. Nicoletti, A. Perucchi, L. Fan, P. Metcalf, M. Marsi and S. Lupi, *Phys. Rev. B: Condens. Matter Mater. Phys.*, 2015, **91**, 155133.
28 N. Kuroda and H. Fan, *Phys. Rev. B: Solid State*, 1977, **16**, 5003.
29 G. Lantz, B. Mansart, D. Grieger, D. Boschetto, N. Nilforoushan, E. Papalazarou, N. Moisan, L. Perfetti, V. L. Jacques, D. Le Bolloc'h, *et al.*, *Nat. Commun.*, 2017, **8**, 13917.
30 B. Mansart, D. Boschetto, S. Sauvage, A. Rousse and M. Marsi, *Europhys. Lett.*, 2010, **92**, 37007.
31 O. Misochko, M. Tani, K. Sakai, K. Kisoda, S. Nakashima, V. Andreev and F. Chudnovsky, *Phys. Rev. B: Condens. Matter Mater. Phys.*, 1998, **58**, 12789.
32 A. Levchuk, B. Wilk, G. Vaudel, F. Labbé, B. Arnaud, K. Balin, J. Szade, P. Ruello and V. Juvé, *Phys. Rev. B*, 2020, **101**, 180102.
33 S. I. Anisimov, B. L. Kapeliovich and T. L. Perel'Man, *J. Exp. Theor. Phys.*, 1974, **39**, 375–377.
34 O. Matsuda and O. Wright, *J. Opt. Soc. Am. B*, 2002, **19**, 3028–3041.
35 J. Winey, Y. Gupta and D. Hare, *J. Appl. Phys.*, 2001, **90**, 3109–3111.
36 W. J. Tropf, M. E. Thomas and T. J. Harris, *Handbook of optics*, 1995, vol. 2, ch. 33.
37 D. Grischkowsky, S. Keiding, M. Van Exter and C. Fattinger, *J. Opt. Soc. Am. B*, 1990, **7**, 2006–2015.
38 W. Yelon and J. Keem, *Solid State Commun.*, 1979, **29**, 775–777.
39 M. M. Qazilbash, A. A. Schafgans, K. S. Burch, S. J. Yun, B. G. Chae, B. J. Kim, H. T. Kim and D. N. Basov, *Phys. Rev. B: Condens. Matter Mater. Phys.*, 2008, **77**, 115121.
40 H. Keer, D. Dickerson, H. Kuwamoto, H. Barros and J. Honig, *J. Solid State Chem.*, 1976, **19**, 95–102.
41 D. Schick, M. Herzog, A. Bojahr, W. Leitenberger, A. Hertwig, R. Shayduk and M. Bargheer, *Struct. Dyn.*, 2014, **1**, 064501.
42 Y. Kalcheim, C. Adda, P. Salev, M.-H. Lee, N. Ghazikhanian, N. M. Vargas, J. del Valle and I. K. Schuller, *Adv. Funct. Mater.*, 2020, **30**, 2005939.
43 J.-P. Fouque, J. Garnier, G. Papanicolaou and K. Solna, *Wave Propagation and Time Reversal in Randomly Layered Media*, Springer Science & Business Media, 2007, vol. 56.